Front. Phys. 10, 100504 (2015)
DOI 10.1007/s11467-015-0466-0

RESEARCH ARTICLE

Experimental system of coupled map lattices

Yu-Han Ma*, Lan-Qing Huang*, Chu-Min Sun*, Xiao-Wen Li†

Department of Physics, Beijing Normal University, Beijing 100875, China

Corresponding author. E-mail: †xwli@bnu.edu.cn

Received December 15, 2014; accepted February 6, 2015

We design an optical feedback loop system consisting of a liquid-crystal spatial light modulator (SLM), a lens, polarizers, a CCD camera, and a computer. The system images every SLM pixel onto one camera pixel. The light intensity on the camera pixel shows a nonlinear relationship with the phase shift applied by the SLM. Every pixel behaves as a nonlinear map, and we can control the interaction of pixels. Therefore, this feedback loop system can be regarded as a spatially extended system. This experimental coupled map has variable dimensions, which can be up to 512 by 512. The system can be used to study high-dimensional problems that computer simulations cannot handle.

Keywords coupled map lattices, photoelectric feedback loop

PACS numbers 05.45.Ra, 05.45.-a, 05.45.Jn, 85.60.-q

1 Introduction

In the field of nonlinear dynamics, partial differential equations are usually used in the study of spatiotemporal systems — time, space, and state variables change continuously, but the inherent limitations of partial differential equations result in serious difficulties in the study. Therefore, in 1992, Kaneko proposed the coupled map lattice (CML) system, a nonlinear dynamical system that is discrete in space and time but maintains continuous state variables [1–4]. The application of the CML system not only overcomes the shortcomings of partial differential equations but also results in a relatively high computing efficiency. Therefore, it is an effective tool for the study of nonlinear systems. The CML system was originally proposed to study spatiotemporal chaos [5], pattern dynamics [3], and complex network problems [6]. With deeper research, the CML system has rapidly developed and is now widely used in various fields, such as population models [7], chemical reactions, biological networks, and encrypted communication [8]. Therefore, the CML system is of great value. In a typical study, computers are used to simulate CML systems, but computer-based simulation systems are limited by the speed of the computer's operation, and the limitation of the system becomes more obvious as the dimensions increase. The experimental system presented in this paper overcomes this limitation.

In this study, we design an experimental CML system that has dimensions of up to 512 by 512. The system contains a photoelectric feedback loop consisting of a liquid-crystal spatial light modulator (SLM), a lens, polarizers, a CCD camera, and a computer. Although computer simulation can solve most CML problems, it is important to handle high-dimensional systems.

This paper is organized as follows. In Section 2, we introduce the experimental setup and model the feedback loop. In Section 3, we study the dynamics of the system experimentally and theoretically. In Section 4, we discuss possibilities for further research and other application of this system.

2 Experimental setup and model

Our experimental system contains a liquid-crystal SLM, a lens, polarizers, a CCD camera, a computer, and a laser (635 nm). Figure 1 shows the experimental setup of the system.

Collimated 635-nm light from a laser passes through a polarizer oriented 45° to the long axis of the SLM. The SLM reflects the light with a relative phase shift between the fast and slow axes. The reflected light passes through another polarizer also oriented 45° to the long axis of the SLM. Then, it passes through the lens before it illuminates the camera. We employ the computer-controlled SLM to apply arbitrary and spatially dependent phase

* These authors contributed equally to this work.

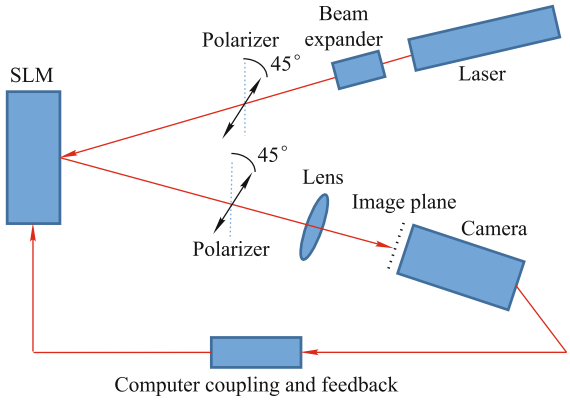

Fig. 1 Experimental setup

modulation to the optical wavefront by using a birefringent liquid crystal sandwiched between an array of reflective electrodes and a transparent cover glass. Each of the electrodes acts as an independent pixel that can impose an arbitrary phase shift ranging from 0 to 2π between the two polarization components of the incoming light by applying an electric field to reorient the liquid crystal. The electric-field component of the incident light linearly polarized at 45° is $\frac{E_0}{2}\binom{1}{1}$. The Jones matrix of the liquid crystal with a vertical slow axis is $\begin{pmatrix} e^{-i\varphi} & 0 \\ 0 & 1 \end{pmatrix}$, and the matrix of the second polarizer is $\frac{1}{2}\begin{pmatrix} 1 & 1 \\ 1 & 1 \end{pmatrix}$. Thus, the electric field of the light illuminating the camera is

$$\begin{aligned} \boldsymbol{E} &= \frac{1}{2}\begin{pmatrix} 1 & 1 \\ 1 & 1 \end{pmatrix}\begin{pmatrix} e^{-i\varphi} & 0 \\ 0 & 1 \end{pmatrix}\frac{E_0}{2}\begin{pmatrix} 1 \\ 1 \end{pmatrix} \\ &= \frac{E_0}{2\sqrt{2}}\begin{pmatrix} \cos\varphi + 1 & -i\sin\varphi \\ \cos\varphi + 1 & -i\sin\varphi \end{pmatrix}. \end{aligned} \tag{1}$$

Therefore, the intensity of light incident on the camera is

$$I = |\boldsymbol{E}|^2 = \frac{E_0^2}{2}(1+\cos\varphi) = \frac{I_0}{2}(1+\cos\varphi). \tag{2}$$

The polarization optics creates a nonlinear relationship between the phase shift φ applied by the SLM and the intensity of light incident on the camera.

We use the light intensity I as a feedback signal to address the SLM and choose an appropriate lookup table such that the phase shift φ is proportional to the light intensity:

$$\varphi = 2\pi I. \tag{3}$$

Then, the light intensity has a nonlinear relationship with the light intensity of last moment:

$$I_{n+1} = \frac{I_0}{2}[1+\cos(2\pi I_n)]. \tag{4}$$

Figure 2 shows this relationship clearly.

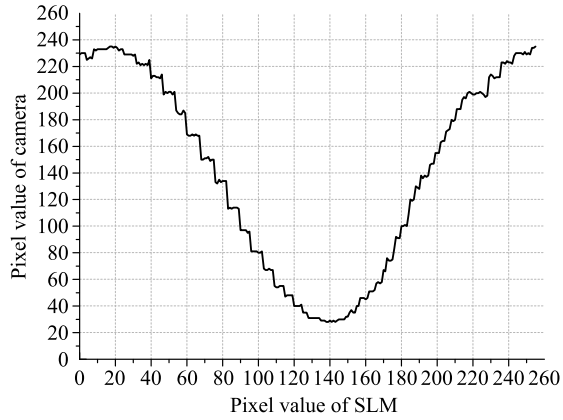

Fig. 2 The relationship between the pixel value of the camera (I_{n+1}) and the pixel value of SLM (I_n).

For each pixel, we are able to acquire a figure similar to Fig. 2. In the setup, we use a lens to image every SLM pixel onto one camera pixel. The SLM we used has 512×512 pixels. We construct a network of iterated maps by using a computer to link the camera and SLM. Each pixel of the SLM or camera corresponds to a node in the network of coupled maps. The dimension of such a CML can be up to 512×512. Feedback is achieved by iteratively updating the phase applied by each pixel on the SLM that depends on the intensity measured by the camera.

3 Dynamics

Figure 3 shows the experimental bifurcation diagram and the largest Lyapunov exponent calculated from the experimental data. Here, k is equivalent to I_0.

We notice the bifurcation behavior from a fixed point to the period-two cycle, then period-four cycle, and

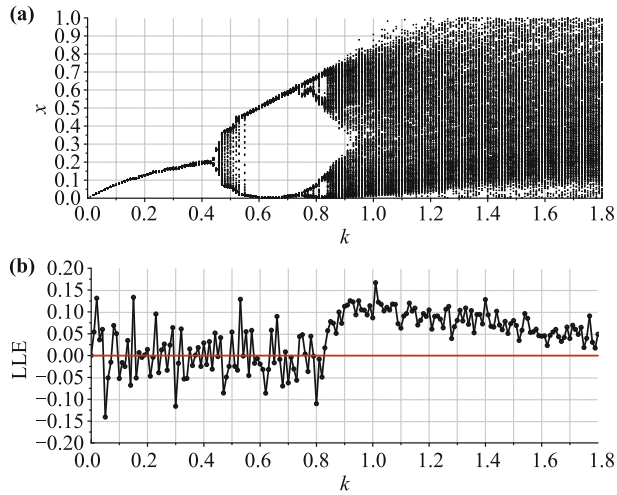

Fig. 3 Experimental results of one pixel. **(a)** Bifurcation diagram of x; **(b)** The largest Lyapunov exponent (LLE) vs. k.

finally a chaotic state. The system undergoes period-doubling routes to chaos.

When $k > 0.84$, the value of largest Lyapunov exponent is greater than zero. We are able to determine that the system reaches chaos when $k > 0.84$. However, it must be noted that when k ranges from 0 to 0.84, the largest Lyapunov exponent is not always less than zero. Aside from obvious acts with intermittent chaos corresponding to the k value, the largest Lyapunov exponent fluctuates near zero, which might originate from the defects of the Kantz algorithm in time-series analysis [9].

Figure 4 shows the simulation result of the map

$$x_{n+1} = \frac{k}{2}[1 + \cos(2\pi x_n)]. \tag{5}$$

Figure 5 shows the simulation result of the bifurcation diagram again in a larger scale and without normalization. On carefully studying the bifurcation diagram, we find that a regular curve is formed by the dense points.

We also find that inside the bifurcation for $k > 0.5$, when $x = k$, the points are densely distributed. When k is equal to half-integer, the points are also distributed densely at $x = 0$.

In order to explain why more points can be found in

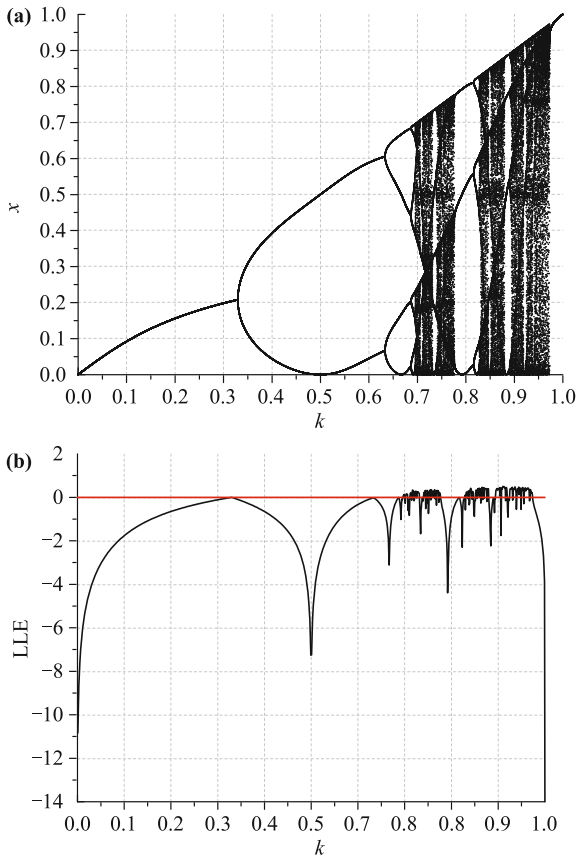

Fig. 4 Simulation results of Eq. (5). **(a)** Bifurcation diagram of x; **(b)** The largest Lyapunov exponent (LLE) vs. k.

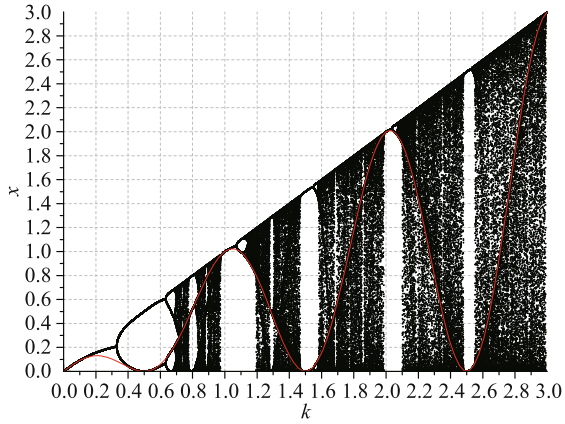

Fig. 5 The dense distribution curve.

some areas and why points are not evenly distributed at each value of k, we study the distribution laws of Eq. (5).

We choose n initial conditions $x(0)$, which are evenly distributed from 0 to 1. After one iteration, we acquire n states $x(1)$.

The value of $y = 1+\cos(2\pi x)$ ranges from 0 to 2 while the range of $x(1)$ is from 0 to k. Because y is not a linear function, the distribution probability of $x(1)$ is no longer even from 0 to k. When $x(1) = 0$ or $x(1) = k$, the absolute value of the slope of y is 0. Therefore, $x(1)$ has the highest probability distribution around 0 or k.

We substitute k into Eq. (5) to obtain $x(2) = \frac{1}{2}k[1 + \cos(2\pi k)]$. This implies that the solution $\frac{1}{2}k[1+\cos(2\pi k)]$ has the highest distribution probability after the second iteration.

On generalizing the derivation above, we obtain the curve $x = \frac{1}{2}k[1 + \cos(2\pi k)]$ in the bifurcation diagram, as shown by the red line. Based on the above derivation, we conclude that the state $x = 0$ will transit to $x = k$ and that the state $x = k$ will transit to $x = \frac{1}{2}k[1+\cos(2\pi k)]$.

Some special values of k help us comprehend and verify this conclusion intuitively.

When $k = \frac{2m+1}{2}$, $x = \frac{1}{2}k[1 + \cos(2\pi k)] = \frac{1}{2}k[1 + \cos(\pi(2m + 1))] = 0$. This implies that around the area $k = \frac{2m+1}{2}$, the solution oscillates between $x = 0$ and $x = k$, as we see the period-two windows around $k = 0.5$, 1.5, and 2.5.

When $k = m$, $x = \frac{1}{2}k[1 + \cos(2\pi m)] = k$, $x = k$ is a fix point when $k = m$. We can see this phenomenon in Fig. 5 at $k = 1, 2, 3$.

Of course, when k is neither an integer nor a half-integer, the solution is not fixed or oscillatory. Therefore, the solutions are distributed from 0 to k. Based on the above analysis, there are three areas, $x = k$, $x = 0$, and $x = \frac{1}{2}k[1 + \cos(2\pi k)]$, where the solutions are densely distributed.

This is why we can see the regular curve inside the

bifurcation diagram.

However, we cannot observe these regular curves from the experimental results. We know that the radical reason why some solutions distribute densely is the characteristic of $\cos(x)$. Furthermore, the solutions being densely distributed at $x = 0$ and $x = k$ will lead to the fact that the solutions are densely distributed at $x = \frac{1}{2}k[1 + \cos(2\pi k)]$. In our experiment, we use a CCD camera to obtain the gray scale of the reflected light. There is hardly any pixel value that is exactly 0. Therefore, we cannot see the period windows and the regular curve $\frac{1}{2}k[1 + \cos(2\pi k)]$.

Figure 6 shows the dynamics of a coupled ring,

$$x_{n+1}(i) = (1-\varepsilon)f(x_n(i)) + \varepsilon f(x_n(i-1)), \quad (6)$$

$$i = 1, 2, \ldots, N,\ x_n(i+N) = x_n(i). \quad (7)$$

Figure 6(a) shows simulation results of state x of a node i vs. the coupling strength ε. Figure 6(b) shows the experimental results of phase φ of node i vs. coupling strength ε. Here $\varphi(i) = 2\pi x(i)$. $f(x_n(i))$ is Eq. (5) with $k = 1.39$ where the local dynamics is chaotic. We can see that the state is chaotic in most coupled regions and periodic in regions where the coupling strength is medium. The experimental result is in good agreement with the simulation.

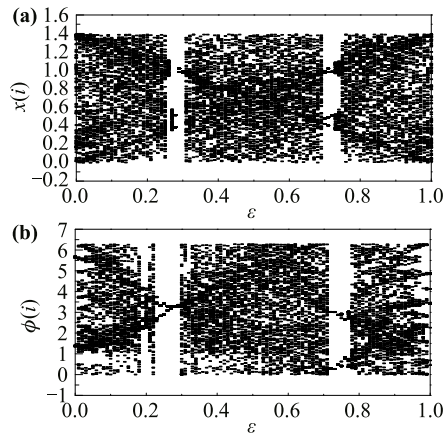

Fig. 6 Simulation and experimental results of a coupled ring Eq. (6). **(a)** Simulation result of $x(i)$ vs. ε. **(b)** Experimental result of $\varphi(i)$ vs. ε. Here $\varphi(i) = 2\pi x(i)$.

4 Further applications

In our experiment, we obtained a CML system filled with 262144 lattices in a 512×512 SLM. We studied the dynamic behavior of a single lattice and a coupled ring theoretically and experimentally. Because we can modify the interaction between lattices, this feedback loop system is actually a complex network with dimensions of up to 512 by 512. Because of the high capacity and rapid response of the optics system, our experimental system shows excellent efficiency compared with computer simulation. As the collective behavior of a complex network is currently a hot topic in nonlinear science [10–12], we are studying this topic by using this experimental CML system. According to our observation, as the coupling strength increases, the coupled map system behaves as cluster synchronization and then global synchronization. We will study the dynamics in more details in the future. We are also studying chimeras in Gaussian-coupled-map lattices. Of course, there are many aspects of the system to be studied. This paper presents the basic dynamic behavior of the system, which forms the foundation for further research on different aspects.

References

1. K. Kaneko, Collapse of Tori and Genesis of Chaos in Dissipative Systems, Vol. 33, World Scientific, 1986
2. K. Kaneko, Lyapunov analysis and information flow in coupled map lattices, *Physica D* 23(1), 436 (1986)
3. K. Kaneko, Pattern dynamics in spatiotemporal chaos: Pattern selection, diffusion of defect and pattern competition intermittency, *Physica D* 34(1), 1 (1989)
4. K. Kaneko, Spatiotemporal chaos in one-and two-dimensional coupled map lattices, *Physica D* 37(1), 60 (1989)
5. G. Hu and Z. L. Qu, Controlling spatiotemporal chaos in coupled map lattice systems, *Phys. Rev. Lett.* 72(1), 68 (1994)
6. P. M. Gade and C.-K. Hu, Synchronous chaos in coupled map lattices with small-world interactions, *Phys. Rev. E* 62(5), 6409 (2000)
7. O. N. Björnstad, R. A. Ims, and X. Lambin, Spatial population dynamics: analyzing patterns and processes of population synchrony, *Trends in Ecology & Evolution* 14(11), 427 (1999)
8. J. Garcia-Ojalvo and R. Roy, Spatiotemporal communication with synchronized optical chaos, *Phys. Rev. Lett.* 86(22), 5204 (2001)
9. H. Kantz, A robust method to estimate the maximal Lyapunov exponent of a time series, *Phys. Lett. A* 185(1), 77 (1994)
10. L. M. Pecora, F. Sorrentino, A. M. Hagerstrom, T. E. Murphy, and R. Roy, Cluster synchronization and isolated desynchronization in complex networks with symmetries, *Nature Communications* 5, 4079 (2014)
11. S. Liu and M. Zhan, Clustering versus non-clustering phase synchronizations, *Chaos* 24, 013104 (2014)
12. M. Zhan, S. Liu, and Z. He, Matching rules for collective behaviors on complex networks: Optimal configurations for vibration frequencies of networked harmonic oscillators, *PLoS ONE* 8(12), e82161 (2013)